Iranian Journal of Medical Physics
Vol. 13, No. 4, December 2016, 228-235
Received: October 23, 2016; Accepted: December 06, 2016

Original Article

Comparison of Two Quantitative Susceptibility Mapping Measurement Methods Used For Anatomical Localization of the Iron-Incorporated Deep Brain Nuclei

Hadis Alvankar Golpaygan[1,2], Mohammad Ali Oghabian[1,2], Seyed Amir Hossein Batouli[1], Arash Zare Sadeghi[1,2]

Abstract

Introduction
Quantitative susceptibility mapping (QSM) is a new contrast mechanism in magnetic resonance imaging (MRI). The images produced by the QSM enable researchers and clinicians to easily localize specific structures of the brain, such as deep brain nuclei. These nuclei are targets in many clinical applications and therefore their easy localization is a must. In this study, we aimed to implement two QSM estimation algorithms, threshold-based k-space division (TKD) and morphology enabled dipole inversion (MEDI) in presurgical planning.
Materials and Methods
In this study, susceptibility weighted imaging (SWI) was performed on six patients referred to our center for presurgical planning purposes. The susceptibility values, as well as the contrast-to-noise ratio of few brain regions were estimated. To identify the algorithm, which was best applicable to clinics, a comparison of the two methods was performed.
Results
QSM images were produced; however, the results did not show any significant differences between the susceptibility values of the two methods. The contrast-to-noise ratio for the susceptibility values of the subthalamic nucleus and substantia nigra brain regions were significantly superior using the MEDI approach over TKD, suggesting improved localization of brain regions using the former method.
Conclusion
This study suggests that to identify specific brain regions, such as deep brain nuclei, a QSM contrast would be more beneficial than the conventional MRI contrasts. This study compared MEDI and TKD methods for quantification of brain susceptibility maps, and results showed that the MEDI method resulted in higher-quality images.

Keywords: Quantitative Measurement, Magnetic Resonance Imaging, Basal Nuclei

[1] *Neuro Imaging and Analysis Group (NIAG), Research Center for Molecular and Cellular Imaging (RCMCI), Tehran University of Medical Sciences, Tehran, Iran*
[2] *Department of Medical Physics and Biomedical Engineering, Faculty of Medicine, Tehran University of Medical Science, Tehran, Iran*
*Corresponding author: Tel: +98 21 66907518; Fax: +98 21 66581533; Email: Oghabian@sina.tums.ac.ir

1. Introduction

Conventional MRI contrasts such as T1- or T2-weighted images are routinely used in clinical applications; however, the contrast of these images may not be appropriate for some specific applications or diagnoses. Therefore, providing images with a contrast based on other less implemented properties of the tissue would be an advantage. Intrinsic properties of brain tissue is, different to its T1 or T2 relaxation times and, is the magnetic susceptibility of the tissue [1], which is the amount of reaction the tissue has to an external magnetic field. Some of the tissues in the body, when supplied with iron-containing compounds, have a special magnetic susceptibility that is different from the surrounding tissue and structures.

Deep brain nuclei have been reported to include iron [2,3], and the amount of iron deposit in these regions has been used as a marker in the diagnosis of many disorders such as Parkinson's, Huntington's [4,5], Alzheimer's disease [6-8], as well as multiple sclerosis [8]Due to the iron deposit in the deep brain nuclei, their measurement of susceptibility would result in considerable contrast with the surrounding structures that had different amounts of iron or other magnetic elements.

Quantitative susceptibility mapping (QSM) is a contrast-enhanced magnetic resonance imaging (MRI) to quantify tissue's magnetic susceptibility [2,9,10], by providing three-dimensional susceptibility distribution maps. These maps are able to illustrate even small susceptibility differences between the adjacent tissues, which help localize brain structures more effectively.

QSM is an inverse problem, and a number of methods have been suggested for estimating QSM. These include calculation of susceptibility through multiple orientation sampling (COSMOS) [11], Threshold-based K-space division (TKD) [12], morphology enabled dipole inversion (MEDI) [13], and homogeneity enabled incremental dipole inversion (HEIDI) [10] algorithms. However, there are some limitations in each of these methods. COSMOS method needs data acquisition from multiple orientations and therefore the patient's head needs to be secured in an uncomfortable position, which makes it inconvenient for clinical applications [11]. HEIDI algorithm uses several different parameters to reconstruct the QSM images, and determination of the optimal values for these parameters are very complicated [10]. The TKD method also provides quantitative susceptibility maps, in which streaking artifacts were apparent [14]. In this study, we aimed to implement two QSM algorithms, MEDI and TKD, in presurgical planning, which is a clinical application of MRI, to localize deep brain nuclei more effectively. These methods were also compared with each other to identify the method best applicable for clinical purposes.

2. Materials and Methods

2.1. MRI data

This study used data from a study performed at the Neuroimaging and Analysis Group (NIAG), Imam Khomeini Hospital, Tehran, Iran. The dataset included Susceptibility Weighted Images (SWI) of six patients with brain lesions (3 Male /3 Female, total mean age: 33±9 years) that were scanned using the same scanner; we applied the same imaging protocols for this purpose.

The scanner was a 3 Tesla (3T) MRI system (Tim Trio, Siemens Medical Solutions) with a 32-channel head coil. Whole brain coronal SWI images were obtained using multi-echo gradient echo sequences with field of view (FOV)= 24 cm^2, repetition time (TR)= 52 ms, flip angel (FA) = 15º, voxel size= 0.94×0.94×2 mm^3, multiple echo times (TEs)= 4.1/ 8.5/ 12.9/ 17.3/ 21.7/ 26.1/ 30.5/ 34.9/ 39.3 ms, and number of average= 1. This protocol lasted 14 min and 29 s.

2.2. MRI data processing

The workflow to generate QSM images from the raw MRI scans included the following four steps: phase unwrapping, generating a binary mask, background field removal, and dipole inversion, which were all performed in MATLAB (version 2013a, The Math Works, Natick, MA).

I) Wrapped phased images: when the values of the voxels of an image are in a range larger

than 2π, the phase image will contain artificial discontinuities, and use of a phase unwrapping algorithm can eliminate these discontinuities [15-17]. A 3D Laplacian-based phase unwrapping algorithm is a fast algorithm, which was used here [16].

II) Creating a binary mask to determine the region of interest is necessary for the following steps [18]. The mask is defined as the largest contiguous region that had an appropriate SNR [19].

III) The magnetic susceptibility sources outside the given region of interest (ROI) usually create a background field; however, generating QSM only requires susceptibility measures from inside the ROI. Background contributions were excluded here using the projection onto dipole fields (PDF) method, which uses the projection theorem in Hilbert space [20].

IV) The last step, dipole inversion, is aimed to estimate the QSM. As mentioned previously, some available methods for QSM estimation such as COSMOS and HEIDI have limitations in clinical applications; however, other methods such as MEDI and TKD have been suggested to be the most applicable methods for QSM estimation in clinics [12,13]. We initially implemented the MEDI algorithm [13]. MEDI requires data acquisition with only one orientation and it generates QSM according to structural consistency between the susceptibility map and the magnitude image. This method reduces streaking artifact using a weighted L1 norm (WL1) minimization, which is an iterative method to solve WL1 using Lagrange multiplier formulation [21]. Choosing an appropriate value for Lagrange multiplier parameter (λ) is crucial to obtain high image quality. Details of the algorithm have been explained previously [13]. The TKD method was also implemented to estimate the QSM [22]. This method considers a threshold (T) to solve the inverse problem, and selecting a proper value for T is necessary to avoid streaking artifacts. Figure 1 shows the estimated workflow of QSM in both methods.

2.3. MRI data analysis

After estimation of the QSM, some brain structures were selected for the susceptibility measures. . We selected substantia nigra (SN), red nucleus (RN), globus pallidus (GP), putamen (Put), and subthalamic nucleus (STN), as they have been suggested in previous work [2,3] to obtain higher iron storage than other brain structures. This feature in these regions enables them to be used as markers for diagnosis of some diseases such as multiple sclerosis, Parkinson's, Huntington's, and Alzheimer's disease. A neuroanatomist manually drew the ROIs for each of the above-mentioned regions on the quantitative susceptibility maps, and the mean susceptibility values of all the voxels within each ROI were calculated.

Because QSM provides estimates of relative susceptibility values, the susceptibility of our ROIs were measured relative to the susceptibility of the white matter (WM), which was used here as a reference. A similar approach was applied to the QSM of both the MEDI and TKD approaches. In addition, using the equation [1], the contrast-to-noise ratio (CNR) of the selected brain structures was estimated (CNR of the STN and SN was selected to qualitatively compare the two methods, because these regions are contiguous and image contrast depends on distinguishing them from each other):

$$CNR = \frac{Mean_{SN} - Mean_{STN}}{std_{(SN,STN)}} \quad (1)$$

Finally, a Wilcoxon rank sum test was performed in SPSS, version 23, to estimate any significant differences between the susceptibility measures of the MEDI and TKD methods.

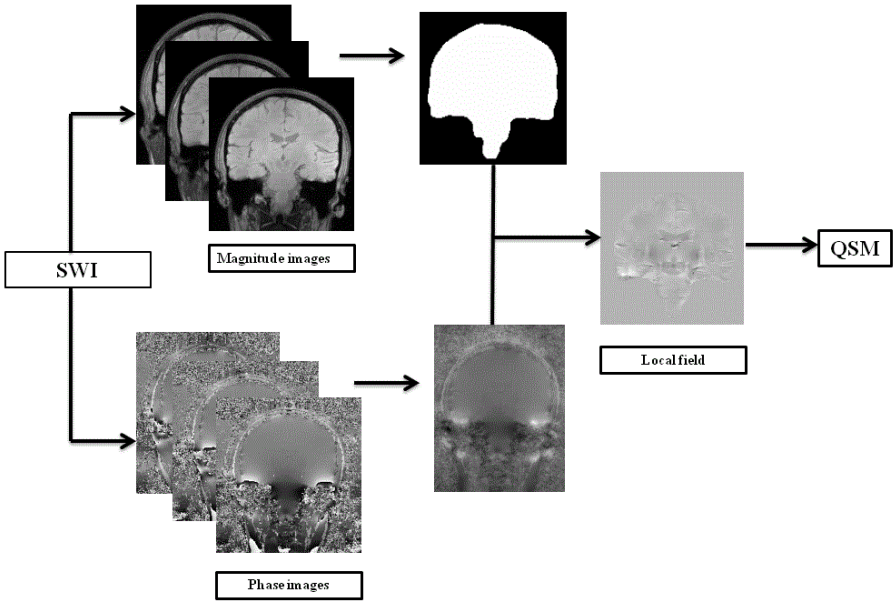

Figure 1. A flowchart of the QSM estimation method

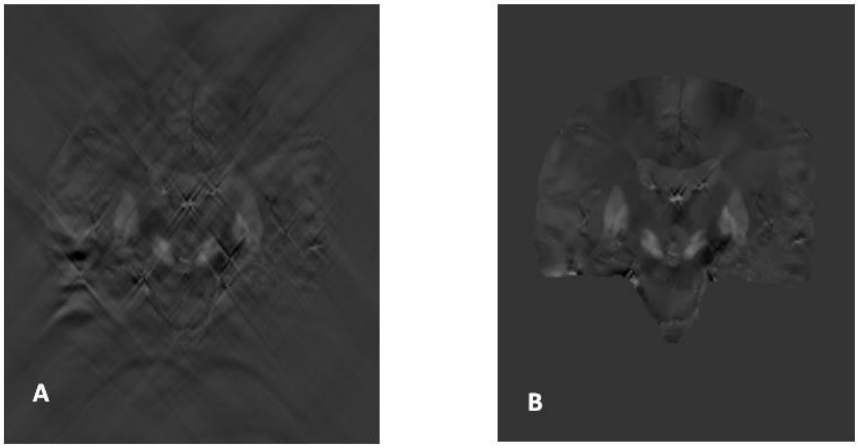

Figure 2. A visual comparison of the A) TKD QSM and B) MEDI QSM. The TKD QSM image intensity was not able to discriminate between the background and brain tissue because there are a lot of streaking artifacts at the image. But at the MEDI QSM image there is a clear border well separated background from the brain tissue because it could well remove streaking artifact.

3. Results

The QSM maps obtained using the MEDI and TKD methods are provided in Figure 2. The MEDI QSM was obtained using λ=900 and the number of iterations in the WL1 method to achieve the final answer were between six and eight iterations. A visual comparison of the two methods shows better quality of the QSM using the MEDI approach. As observed in Figure 3, deep brain nuclei are clearly evident on a MEDI map compared to a conventional T1 scan, revealing the importance of using QSM method for visualization and localization of the brain nuclei.

Susceptibility values of the selected brain regions using both methods are provided in Table 1. Similar estimations are observed for the susceptibility values of brain regions in both methods, and further analysis revealed no statistically significant differences between the outputs of these methods (P>0.05).

By estimating the CNR of the STN and SN brain regions, we further compared the quality of the QSM between the two methods; higher CNR indicates better image quality. The results showed a significantly (P=0.018) higher CNR for the MEDI approach compared to TKD (0.84 (CNR of the MEDI) >0.35 (CNR of the TKD)),

suggesting that better quality QSM images were obtained using this method.

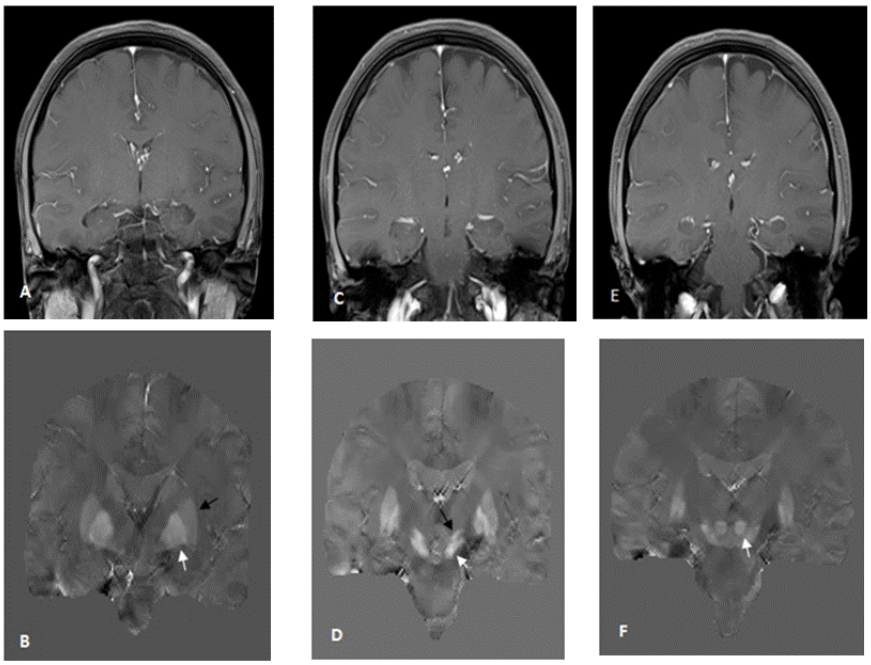

Figure 3: The deep brain nuclei observed in a MEDI QSM compared to a conventional T1 scan in the same section of the brain. A, C and E) conventional T1: There is no clear evidence of deep brain nuclei. B, D and F) MEDI QSM from the same sections of the brain. Putamen (black arrow) and Globus pallidus (white arrow) in B, Subthalamic nucleus (black arrow) and Substantia nigra (white arrow) in D and red nucleus (white arrow) in F are clearly seen.

Table 1. Susceptibility values of the selected Regions Of Interest (ROIs) in the TKD and MEDI methods. (Mean ± standard deviation)

ROI	White matter (WM)	Red Nucleus (RN)	Subthalamic Nucleus (STN)	Substantia Nigra (SN)	Globus Pallidus (Gp)	Putamen (Put)
$\Delta\chi_{MEDI}$	$-0.01^{\pm}$ 0.002	$0.12^{\pm}$ 0.004	$0.09^{\pm}$ 0.009	$0.16^{\pm}$ 0.006	$0.15^{\pm}$ 0.011	$0.08^{\pm}$ 0.01
$\Delta\chi_{TKD}$	$-0.02^{\pm}0.02$	$0.1^{\pm}$ 0.03	$0.11^{\pm}$ 0.03	$0.14^{\pm}$ 0.02	$0.16^{\pm}0.02$	$0.09^{\pm}0.03$

The results indicated that although the processing steps and the time taken by the MEDI and TKD methods do not differ significantly, the QSM images obtained using the former approach had higher quality, suggesting MEDI to be the algorithm that is more applicable for clinical purposes.

4. Discussion

In this study, we aimed to reconstruct QSM images, which are useful to improve visualization of deep brain nuclei, in comparison with conventional T1- or T2-weighted images. The QSM images were reconstructed here using the two algorithms of MEDI and TKD, and the accuracy of the susceptibility maps obtained by these two methods were also compared. We observed better quality in the QSM images obtained by the MEDI algorithm, compared to TKD. This was mainly due to the streaking artifacts of the QSM of the TKD, as this could blur the borders of brain regions, resulting in an inadequate anatomy diagnosis.

Despite a better quality of MEDI for QSM, the susceptibility values obtained using the two methods did not differ significantly, suggesting applicability of both methods to evaluate susceptibility measures of brain tissue. Despite similar susceptibility measures, the CNR for the susceptibility values of the STN and SN brain regions were significantly superior using the MEDI approach over the TKD, which is in contrast to the similar susceptibility values of the two methods. This could be explained by the different levels of residual noise in the two approaches. Therefore, for a quantitative assessment, MEDI and TKD methods do not differ significantly, the MEDI approach is suggested for a more accurate visualization of brain anatomy.

An important application of this study is to quantify specific biomarkers, such as iron in different brain regions, as the level of this biomarker, particularly in deep brain nuclei, would be beneficial for the diagnosis of some diseases and disorders. A postmortem study by Chen et al. [4] showed that putamen samples from Huntington and Parkinson's patients increased several-fold in iron concentration compared with normal brains. This could be configured using QSM; furthermore, a higher susceptibility would mean a higher level of iron concentration. This approach could also be used for early detection of diseases, examples include earlier detection of Huntington's disease in those individuals who are genetically prone through estimation of the susceptibility measurements of the candidate's brain regions.

Similarly, the susceptibility measurements of other brain regions such as substantia nigra, red nucleus, and subthalamic nucleus would also be markers for the diagnosis of diseases. Examples of abnormal susceptibility measurements of brain regions in different diseases include a deposition of iron at putamen and a caudate in Huntington's disease [23], at putamen, subthalamic nucleus, as well as globus pallidus in Parkinson's disease and multisystem atrophy variants [24-27] in the whole cerebral cortex in Alzheimer's disease [7] and adjacent to plaques in multiple sclerosis [28]. QSM images also help with anatomical localization of the deep brain nuclei, such as subthalamic nucleus, which is the target in many deep brain stimulation applications [29].

5. Conclusion

This study compared two methods for quantification of brain susceptibility maps, and illustrated that both methods were able to detect the susceptibility measures, although one method resulted in higher-quality images. The QSM method had some strength over the conventional T1 or T2-weighted methods. Consequently, susceptibility is a fundamental property of the tissues, and therefore, the resulting QSM images are less influenced by those confounding factors that affect the quality of conventional MRI images.

Despite the strengths, this study was limited in measuring the relative susceptibility measures, not the absolute values. Also, as the aim of the study was to measure the susceptibility of brain tissues, we used a multi-echo gradient-echo sequence with nine echo times, from low to high. However, for measuring the susceptibility of other tissues, different echo times may be needed to implement, as short echo times are used to determine tissues with high-susceptibility values and long echo times can determine tissues with lower susceptibility values

This study demonstrated that QSM is necessary for better visualization of specific deep brain regions, as well as for diagnosis or early-detection of some diseases and disorders. Exploration of a method that converts the susceptibility measures estimated in a QSM to the absolute iron concentration in a tissue is recommended for future work.

Acknowledgements

This study was financially supported by a grant from Tehran University of Medical Sciences (Grant ID. 21706).

References

1. Haacke E M,Mittal S,Wu Z,Neelavalli J and Cheng Y-C. Susceptibility-weighted imaging: technical aspects and clinical applications, part 1. AJNR. 2009; 30(1):19-30. DOI: 10.3174/ajnr.A1400.
2. Langkammer C,Schweser F,Krebs N,Deistung A,Goessler W,Scheurer E,Fazekas F. Quantitative susceptibility mapping (QSM) as a means to measure brain iron? A post mortem validation study. NeuroImage. 2012; 62(3):1593-9. DOI: http://dx.doi.org/10.1016/j.neuroimage.2012.05.049.
3. Schweser F,Deistung A,Lehr B W and Reichenbach J R. Quantitative imaging of intrinsic magnetic tissue properties using MRI signal phase: an approach to in vivo brain iron metabolism? NeuroImage. 2011; 54(4):2789-807. DOI: http://dx.doi.org/10.1016/j.neuroimage.2010.10.070.
4. Chen J C,Hardy P A,Kucharczyk W,Clauberg M,Joshi J,Vourlas A,Henkelman R. MR of human postmortem brain tissue: correlative study between T2 and assays of iron and ferritin in Parkinson and Huntington disease. AJNR. 1993; 14(2):275-81.
5. Dexter D,Carayon A,Javoy-Agid F,Agid Y,Wells F,Daniel S,Marsden C. Alterations in the levels of iron, ferritin and other trace metals in Parkinson's disease and other neurodegenerative diseases affecting the basal ganglia. Brain. 1991; 114(4):1953-75. DOI: https://doi.org/10.1093/brain/114.4.1953.
6. Bouras C,Giannakopoulos P,Good P F,Hsu A,Hof P and Perl D. A laser microprobe mass analysis of brain aluminum and iron in dementia pugilistica: comparison with Alzheimer's disease. Eur Neurol. 1997; 38(1):53-8. DOI: 10.1159/000112903.
7. Hallgren B and Sourander P. The non-haemin iron in the cerebral cortex in Alzheimer's disease J Neurochem. 1960; 5(4):307-10.
8. LeVine S M. Iron deposits in multiple sclerosis and Alzheimer's disease brains. Brain Res. 1997; 760(1):298-303. DOI: http://dx.doi.org/10.1016/S0006-8993(97)00470-8.
9. Bilgic B,Pfefferbaum A,Rohlfing T,Sullivan E V and Adalsteinsson E. MRI estimates of brain iron concentration in normal aging using quantitative susceptibility mapping. NeuroImage. 2012; 59(3):2625-35. DOI: http://dx.doi.org/10.1016/j.neuroimage.2011.08.077.
10. Schweser F,Sommer K,Deistung A and Reichenbach J R. Quantitative susceptibility mapping for investigating subtle susceptibility variations in the human brain. NeuroImage. 2012; 62(3):2083-100. DOI: http://dx.doi.org/10.1016/j.neuroimage.2012.05.067.
11. Liu T,Spincemaille P,de Rochefort L,Kressler B and Wang Y. Calculation of susceptibility through multiple orientation sampling (COSMOS): a method for conditioning the inverse problem from measured magnetic field map to susceptibility source image in MRI. Magn Reson Med. 2009; 61(1):196-204. DOI: 10.1002/mrm.21828.
12. Shmueli K,de Zwart J A,van Gelderen P,Li T Q,Dodd S J and Duyn J H. Magnetic susceptibility mapping of brain tissue in vivo using MRI phase data. Magn Reson Med. 2009; 62(6):1510-22. DOI: 10.1002/mrm.22135.
13. Liu J,Liu T,de Rochefort L,Ledoux J,Khalidov I,Chen W,Prince M R. Morphology enabled dipole inversion for quantitative susceptibility mapping using structural consistency between the magnitude image and the susceptibility map. NeuroImages. 2012; 59(3):2560-8. DOI: http://dx.doi.org/10.1016/j.neuroimage.2011.08.082.
14. Wharton S,Schäfer A and Bowtell R. Susceptibility mapping in the human brain using threshold- based k-space division. Magn Reson Med. 2010; 63(5):1292-304. DOI: 10.1002/mrm.22334.
15. Witoszynskyj S,Rauscher A,Reichenbach J R and Barth M. Phase unwrapping of MR images using ΦUN–a fast and robust region growing algorithm. MED IMAGE ANAL. 2009; 13(2):257-68. DOI: http://dx.doi.org/10.1016/j.media.2008.10.004.
16. Schofield M A and Zhu Y. Fast phase unwrapping algorithm for interferometric applications. OPT LETT. 2003; 28(14):1194-6. DOI: https://doi.org/10.1364/OL.28.001194.
17. Abdul-Rahman H S,Gdeisat M A,Burton D R,Lalor M J,Lilley F and Moore C J. Fast and robust three-dimensional best path phase unwrapping algorithm. Applied optics. 2007; 46(26):6623-35.
18. Haacke E M,Liu S,Buch S,Zheng W,Wu D and Ye Y. Quantitative susceptibility mapping: current status and future directions. MRI. 2015; 33(1):1-25.
19. Pandian D S,Ciulla C,Haacke E M,Jiang J and Ayaz M. Complex threshold method for identifying pixels that contain predominantly noise in magnetic resonance images. Journal of Magnetic Resonance Imaging. 2008; 28(3):727-35. DOI: 10.1002/jmri.21487.
20. Liu T,Khalidov I,de Rochefort L,Spincemaille P,Liu J,Tsiouris A J and Wang Y. A novel background field removal method for MRI using projection onto dipole fields (PDF). NMR Biomed. 2011; 24(9):1129-36. DOI: 10.1002/nbm.1670.

21. Vogel C R. Computational methods for inverse problems. Vol. 23. 2002: Siam.
22. Yang G. Computing Magnetic Susceptibility Maps from Gradient Recalled Echo MRI for use in Multiple Sclerosis Studies. [thesis], Ohio State university. 2013.
23. Klintworth G K. Huntington's chorea: morphologic contributions of a century. ADV NEUROL. 1973; 1:1872-972.
24. Rojas G,Asenjo A,Chiorino R,Aranda L,Rocamora R and Donoso P. Cellular and Subcellular Structure of the Ventrolateral Nucleus of the Thalamus in Parkinson Disease Deposits of Iron. Stereotact Funct Neurosurg. 1965; 26(3-5):362-76. DOI: 10.1159/000104083.
25. Earle K M. Studies on Parkinson's disease including x-ray fluorescent spectroscopy of formalin fixed brain tissue. J Neuropathol Exp Neurol. 1968; 27(1):1-14.
26. Lhermitte J,Kraus W and McAlpine D. Etude des produits de desintegration et des depots du globus pallidus dans un cas de syndrome parkinsonien. Rev Neurol. 1924; 1:356-61.
27. Borit A,Rubinstein L and Urich H. The striatonigral degenerations. Putaminal pigments and nosology. Brain: J. Neurol. 1975; 98(1):101-12.
28. Craelius W,Migdal M,Luessenhop C,Sugar A and Mihalakis I. Iron deposits surrounding multiple sclerosis plaques. Arch Pathol Lab Med. 1982; 106(8):397-9.
29. Liu T,Eskreis-Winkler S,Schweitzer A D,Chen W,Kaplitt M G,Tsiouris A J and Wang Y. Improved subthalamic nucleus depiction with quantitative susceptibility mapping. Radiology. 2013; 269(1):216-23. DOI: http://dx.doi.org/10.1148/radiol.13121991.